Characterization of Graphene-based Ink for RF Applications

Characterization of Graphene-based Ink for RF Applications

Davide Arcoraci[1], Fabio Peinetti[2], Pietro Zaccagnini[1] and Patrizia Savi[2]

***Abstract*— Carbon based materials (carbon nanotubes, graphene) exhibit interesting physical properties and have been recently investigated in many applications. In the family of carbon allotropes, graphene has attracted particular attention for its exceptional electrical properties. However, graphene as many other carbon based materials, cannot be deposited on substrates in bulk quantities without exploiting solvent casting techniques, by means of inks. In this work, the electrical properties of a graphene-based ink are analyzed. The graphene film is deposited on a gap along a microstrip line with controlled circular pattern geometry. Several prototypes are realized on a RF substrate from Panasonic substrate. The surface impedance of the graphene-based films and their scattering parameters are measured for two different graphene deposition thicknesses. The graphene film is modelled with a lumped element model. The impedance values are used as a first estimation of the sheet impedance in a full-wave analysis.**

I. INTRODUCTION

Graphene is one of the most researched carbon-based materials. It is characterized by valuable properties, ranging from high thermal conductivity to high mechanical strength and to high carrier mobility [1]. Graphene properties have been studied in the fields of electronics and photonics but also in mechanics and buildings [2]–[9].

With a proper solvent, graphene flakes can be dispersed with different binders to produce inks. The inks can be used with various printing methods to produce films. Films can be realized with several techniques such as drop casting [10], epitaxial growth [11], chemical vapor deposition [12], and screen printing techniques [13].

These techniques are expensive and not suitable for mass production. By using proper solvent and binders in order to obtain a film that can be directly doctor-bladed on a dielectric substrate of a device, commercialization and widespread deployment are made possible.

Graphene films have found many applications as sensing element in gas sensors [14], biosensors [15], [16], humidity, temperature and pressure monitoring [17], [18] and tunable device [19]–[23]. Graphene films have been gaining the attention of researcher in the last few years in robot manufacturing for strain, pressure and tactile sensors, skin, arms etc. for cost-effective robots [24], [25].

For these applications it is very important to electrically characterize the used graphene deposition both at low and microwave frequency.

*This work was not supported by any organization

[1]Davide Arcoraci and Pietro Zaccagnini are with Department of Applied Science and Technology (DISAT), Politecnico di Torino,Corso Duca degli Abruzzi 24, 10129 Turin, Italy pietro.zaccagnini@polito.it

[2]Fabio Peinetti and Patrizia Savi are with the Department of Electronics and Telecommunications (DET), Politecnico di Torino, Corso Duca degli Abruzzi 24, 10129 Turin, Italy patrizia.savi@polito.it

In this work, a graphene-based ink is made and manually deposited on a microstrip line printed on a Panasonic R-1566 substrate. The electric properties of the ink are analyzed at microwave frequency so to obtain a circuital model, working in the 500 MHz to 5 GHz range. The impedance of the simulated model is confirmed by the a direct measure of the impedance of the deposition. The surface impedance values obtained with the circuit model analysis are then used as starting point for a full-wave characterization with CST software.

In Section II the ink preparation method and the deposition technique are described into detail. In Section III the impedance of the deposition is measured by means of a frequency response analyzer. The scattering parameters of a reference line and lines with the graphene deposition are evaluated with a vector analyzer. Lumped elements simulations and full-wave simulations are performed and the results compared with the measurements. In Section IV some conclusions are drawn.

II. INK PREPARATION AND DEPOSITION

A. Ink preparation

The graphene-based ink was prepared according to the following procedure. Polyvinylidene Fluoride (PVDF, Kynar® HSV 1800 provied by Imerys) was first dispersed into N-Methyl Pyrrolidone (NMP, provided by Sigma) at 60°C, under stirring conditions, to fasten the dissolution process. The graphene powder (provided by NanoInnova, NIT Graphene Nanoplatelets) have a surface area to weight ratio of 45 m^2/g with a carbon content of 98.9 wt%. Material characterization and detailed description of the graphene nanoplatelets can be found in [26]. The graphene powder was added as soon as the PVDF dispersion became homogeneous. The ink was let stir overnight to guarantee a homogeneous dispersion. The ink formulation was 9:1 in weight graphene powder:PVDF. The amount of solvent was 0.1 mL_{NMP}/mg_{PVDF}.

B. Deposition on a microstrip line

The graphene-based ink is deposited on a microstrip line. The substrate of the line is Panasonic R-1566 (nominal $\epsilon_r = 4.6$, $\tan\delta = 0.012$) of thickness 1.6 mm. The copper layers are 35 micron thick. In order to achieve a $50\ \Omega$ impedance, the line was chosen to be 2.9 mm width. The total length of the line is 60 mm with a gap of 2 mm in the middle. The graphene ink was deposited in the 2 mm gap, ensuring coverage of the copper strip line, guaranteeing physical and electrical contact. (see Fig. 1).

The graphene deposition was realized with a masking process carried out by means of a physical mask made of

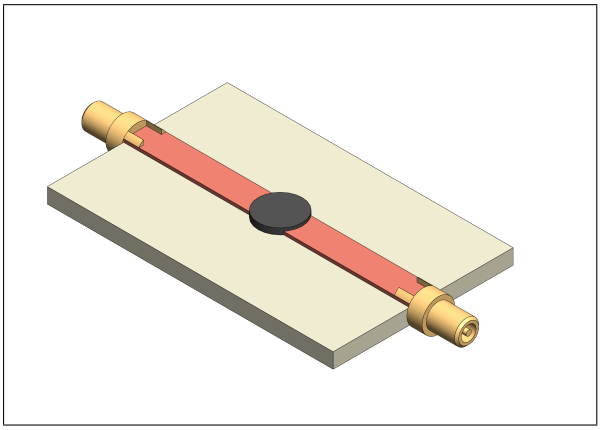

Fig. 1: View of transmission line with the circular graphene film.

adhesive Kapton® mask (75 micron thick) with one or two layers overlapped. In the case of one layer mask, the average thickness of the graphene deposition is 110 micron, whereas in the case of two-layers mask the deposition results to be 190 micron.

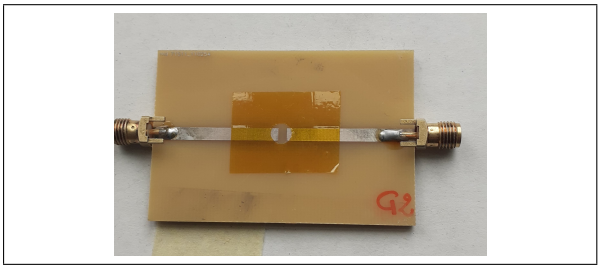

Fig. 2: Adhesive Kapton mask (single layer).

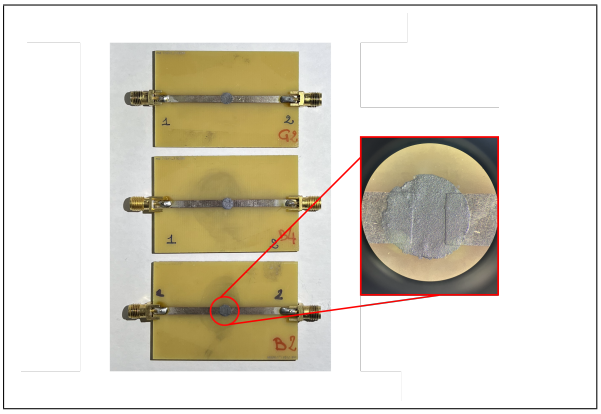

Fig. 3: Microstrip transmission lines with graphene deposition.

III. Results

A. Impedance measurements

Impedance measurements were carried out in the frequency range $[10^6, 10^{-1}]$ Hz by means of a frequency response analyzer (FRA32-M, provided by Metrohm). The amplitude of the probe signal was set to 5 mV and the spectrum was sampled 10 points per decade. In Fig. 4 it is possible to see the frequency response of the three microstrips, B2 and B4 microstrips present a costant impedance across the spectra of respectively $8.2\ \Omega$ and $4.9\ \Omega$. G2 microstrips with doubled layer respect to the first two, present a constant impedance of about $16.4\ \Omega$. The ratio Z_{G2}/Z_{B2} coherent with expected result. The discrepancy with the B4 most probably is due to manual processing errors linked to graphene deposition step. The results are further summarized in Table I

TABLE I: Averages and deviations of the resistance value in the frequency range $[10^4, 10^{-1}]$ Hz.

Sample Name	Nr. Kapton mask layers	$Z_{\text{Mean}}(\Omega)$	$\sigma_{\text{dev}}(m\Omega)$
B2	2	8.3	9.40
B4	2	4.9	5.01
G2	1	16.4	12.20

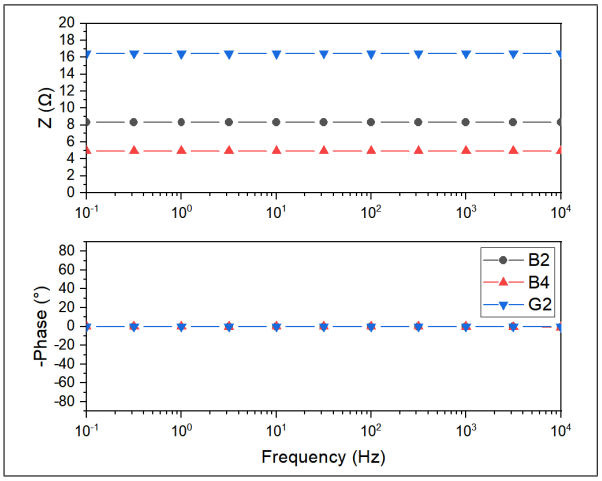

Fig. 4: Impedance measurements: Bode and phase plot.

B. Scattering parameters measurements

The scattering parameters of a reference line (without gap) and of the lines with graphene pad deposited on the gap are measured with a two-port USB vector analyzer (VNA, P9371A) by Keysight, Santa Rosa, CA, USA. in the frequency range 0.1 GHz to 6 GHz. A standard two-port calibration is performed with an E-cal, N7552A, DC - 9 GHz calibration kit.

In Fig. 6 and Fig. 7 the measured scattering parameters are reported. The dotted line represents the reference line without the gap. The other two curves account for graphene-ink filled gap measurements. The frequency decrease in the S_{21} is due to dielectric and copper losses.

From Fig. 6 the transmission coefficient is lower in the case of the double layer Kapton mask graphene deposition (continuous line) with respect to the single layer one (dashed line). Such a phenomena is linked to the graphene deposition thickness and it can be noted that a similar behavior is observed in the reflection coefficient in Fig. 7.

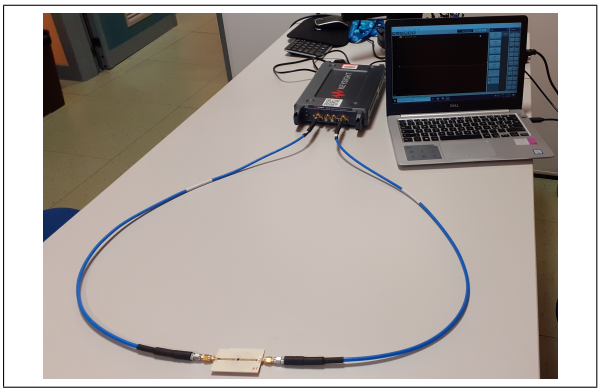

Fig. 5: Measurement setup: a two-port USB vector analyzer by Keysight and the microstrip line with graphene deposition.

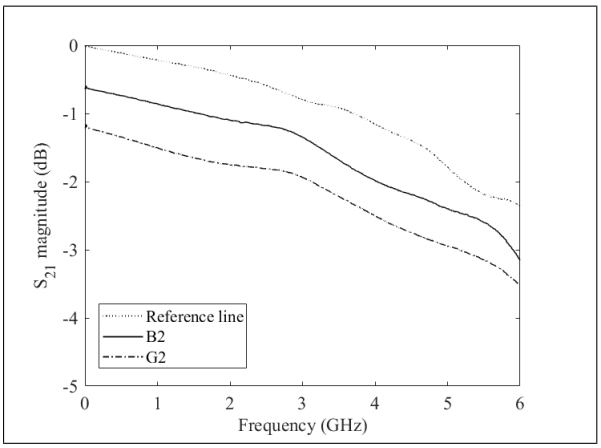

Fig. 6: Measured transmission coefficient of the reference line and graphene depositions with single (G2) and double layer Kapton mask (B2).

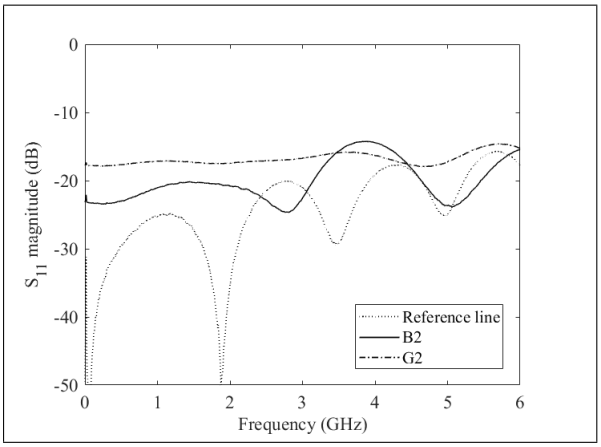

Fig. 7: Measured reflection coefficient of the reference line and graphene depositions with single (G2) and double layer Kapton mask (B2).

In Fig. 8 the transmission coefficients of two graphene depositions, realized with a double layer Kapton mask, are reported. The reproducibility of the measurement is highlighted by the small difference in the S_{21} of the two prototypes. In Fig. 9 the two curves are similar each other. A slight difference could be noted and is probably due to the SMA connector soldering.

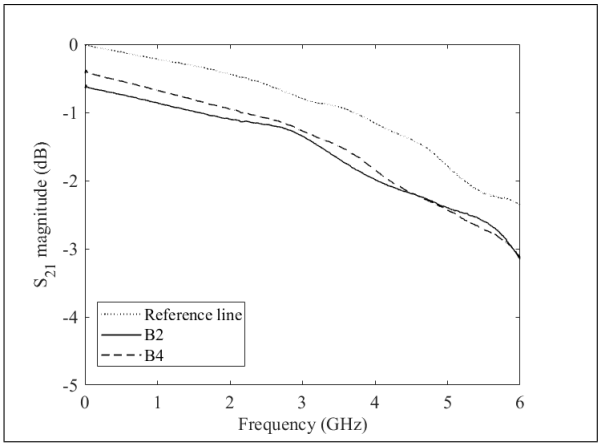

Fig. 8: Comparison between the measured transmission coefficients of two different prototypes with double layer Kapton mask graphene deposition.

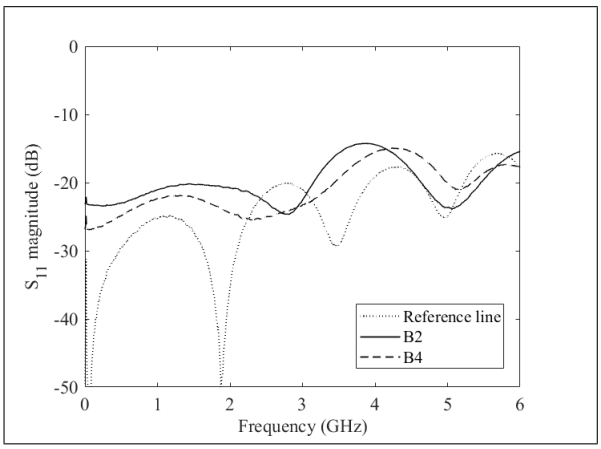

Fig. 9: Comparison between the measured reflection coefficients of two different prototypes with double layer Kapton mask graphene deposition.

C. Lumped-element model

In this section the lumped element model is described. It is developed by fitting the measured scattering parameters, discussed in Sec. III-B. The model was developed by means of ADS software from Keysight and is already reported in several works [27]–[29]. From Fig. 10, the gap is modeled by a capacitance C_p and its loss term R_p. The parasitic capacitances between each line and the ground plane are accounted for by an RC group (C_{in} and R_{in}, C_{gl} and R_{gl} respectively). The resistive element is linked to the dielectric losses. Due to symmetry those components are equal each

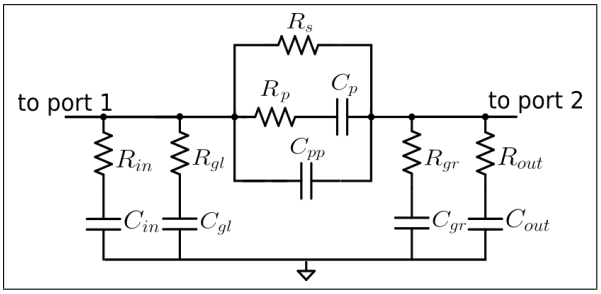

Fig. 10: Lumped circuital model of the deposited graphene film.

other on the two sides of the gap. C_{pp} is due to the formation of nanoscale capacitors among the graphene flakes. R_s is due to the presence of the graphene deposition and it is also the only remaining element at null frequency (DC). The model seems to be able to describe both the single layer and double layer Kapton mask graphene deposition. In order to model the two cases, all the model parameters are left unchanged (see Table II). The parameter that should be changed is R_s that is about $8\ \Omega$ in the case of single layer Kapton mask graphene deposition and about $18\ \Omega$ in the case of double layer Kapton mask graphene deposition.

TABLE II: Lumped model Simulation parameters: single layer Kapton mask and double layer mask graphene deposition.

Parameter (unit)	Value
C_{pp}(pF)	0.07
$R_p(\Omega)$	25.5
C_p(pF)	4.2
$R_{gl}(\Omega)$	193
C_{gl}(pF)	0.1
$R_{gr}(\Omega)$	193
C_{gr}(pF)	0.1
$R_{in}(\Omega)$	193
C_{in}(pF)	0.01
$R_{out}(\Omega)$	193
C_{out}(pF)	0.01

Simulation results and a comparison with the measured scattering parameters are reported in Fig. 11 and Fig. 12 for the graphene deposition with a single layer Kapton mask and in Fig. 13, Fig. 14 for the double layer kapton mask graphene deposition. A good matching between the simulated and the measured curves can be appreciated for both the graphene deposition thickness.

D. Full-wave simulations

Full-wave simulations are performed using CST Studio Suite and compared with the results obtained in the previous sections. The simulations exploit a frequency domain solver with an adaptive meshing refining. In Fig. 15 the simulated geometry is reported.

The substrate of the microstrip is defined as a material with $\epsilon_r = 4.6$ and $\tan\delta = 0.021$ at 2 GHz. The graphene ink deposition is modelled as a flat, round-shaped surface impedance.

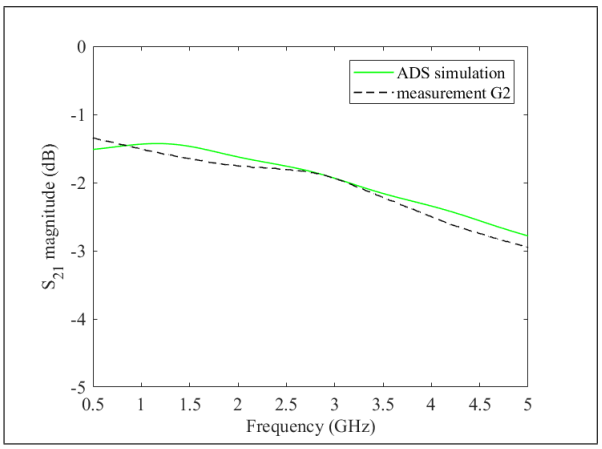

Fig. 11: Measured and simulated Transmission coefficient comparison for a single layer Kapton mask graphene deposition (G2).

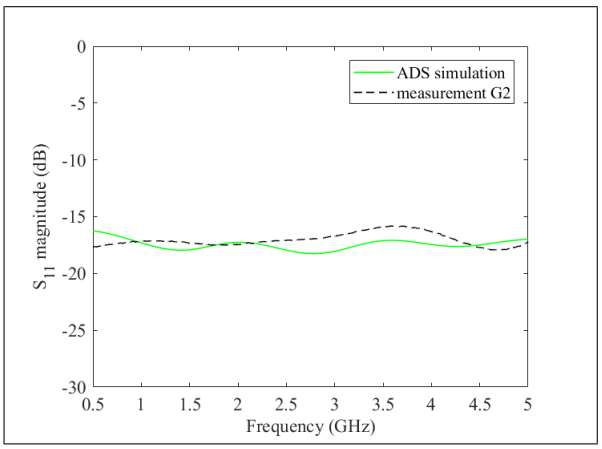

Fig. 12: Measured and simulated reflection coefficient comparison for a single layer Kapton mask graphene deposition (G2).

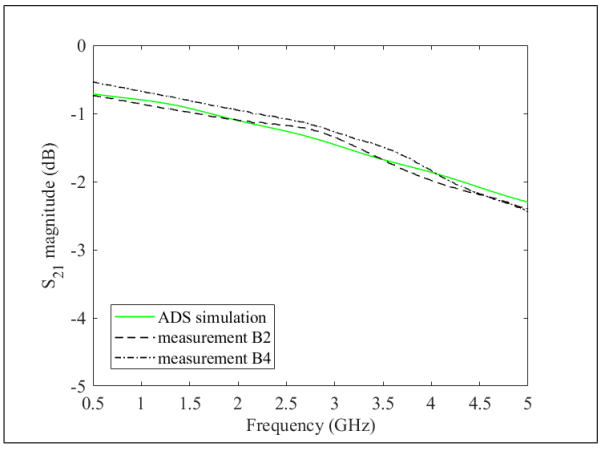

Fig. 13: Measured and simulated Transmission coefficient comparison for double layer Kapton mask graphene depositions (B2, B4).

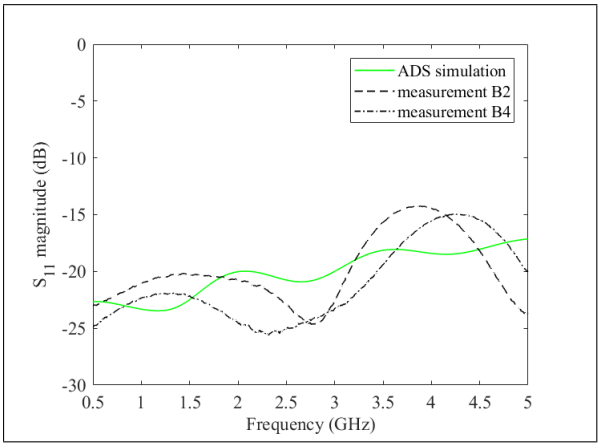

Fig. 14: Measured and simulated Reflection coefficient comparison for double layer Kapton mask graphene depositions (B2, B4).

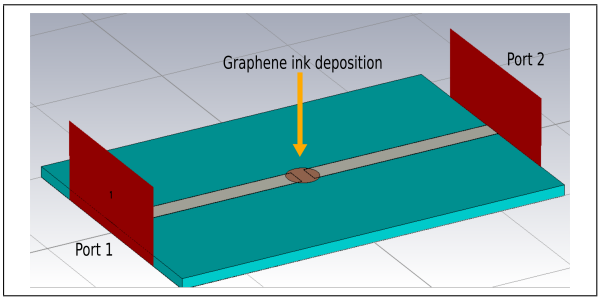

Fig. 15: Geometry for the full-wave simulations

For the double layer Kapton mask graphene deposition $\Re(Z)$ is set to 20 Ω/sq, while for the single layer Kapton mask a 45 Ω/sq impedance was chosen. The imaginary part is zero as suggested from the impedance measurements reported in Sec. III-A. Since the sheet impedance is in Ω/sq it is necessary to convert into Ω for a better comparison with the measured value. Given an aspect ratio of 2/3 (length of the gap over width of the microstrip), the corresponding impedance is 13 Ω and 30 Ω, respectively. Those values are of the same order of magnitude obtained with the impedance measurements (see Sec. III-A) and of ADS simulation (see Sec. III-C).

Full-wave simulation results are reported in Fig. 16 in the frequency range 500 MHz to 5 GHz and compared with the measurements.

IV. CONCLUSIONS

A graphene-based ink to be manually deposited on a microstrip circuit is fabricated. Graphene circular deposition of two different thicknesses (110 μm and 190 μm) are modeled through a lumped-element circuit. Electromagnetic behaviour of both films was simulated with ADS in the 1 GHz to 5 GHz range. The scattering parameters of the microstrip lines with the graphene ink is measured and fitted by means of RC series groups. Simulated and experimental results were found to be in accordance with each other. Also the measured

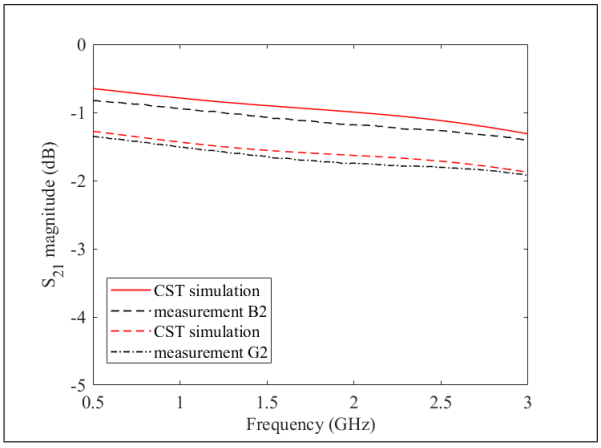

Fig. 16: Measured and Full-wave simulation of transmission coefficient comparison for a single layer Kapton mask graphene deposition (G2) and for a double layer Kapton mask graphene depositions (B2, B4).

impedance provides a further confirmation of the proposed model. This equivalent lumped circuit can be extended to characterize films with different graphene thickness. The circuit model has been used as first step for defining the sheet impedance of full-wave simulations. Graphene depositions used in sensing devices and robots applications can be studied by using the present characterization from DC to high frequency.

REFERENCES

[1] A. K. Geim, "Graphene: status and prospects," *science*, vol. 324, no. 5934, pp. 1530–1534, 2009.

[2] J. Liu, Y. Xue, M. Zhang, and L. Dai, "Graphene-based materials for energy applications," *MRS bulletin*, vol. 37, no. 12, pp. 1265–1272, 2012.

[3] T. Oğuzer and A. Altıntaş, "Evaluation of the e-polarization focusing ability in thz range for microsize cylindrical parabolic reflector made of thin dielectric layer sandwiched between graphene," *IET Microwaves, Antennas & Propagation*, vol. 15, no. 10, pp. 1240–1248, 2021.

[4] F. O. Yevtushenko, S. V. Dukhopelnykov, T. L. Zinenko, and Y. G. Rapoport, "Electromagnetic characterization of tuneable graphene-strips-on-substrate metasurface over entire thz range: Analytical regularization and natural-mode resonance interplay," *IET Microwaves, Antennas & Propagation*, vol. 15, no. 10, pp. 1225–1239, 2021.

[5] H. Lotfalizadeh and M. Ghaffari-Miab, "Dyadic green's function of partially filled graphene-loaded rectangular waveguides," *IET Microwaves, Antennas & Propagation*, vol. 15, no. 14, pp. 1785–1798, 2021.

[6] Z.-C. Lin, Y. Zhang, L. Li, Y.-T. Zhao, J. Chen, and K.-D. Xu, "Extremely wideband metamaterial absorber using spatial lossy transmission lines and resistively loaded high impedance surface," *IEEE Transactions on Microwave Theory and Techniques*, 2023.

[7] Y. Cai, Y. Huang, N. Feng, and Z. Huang, "Improved transformer-based target matching of terahertz broadband reflective metamaterials with monolayer graphene," *IEEE Transactions on Microwave Theory and Techniques*, 2023.

[8] V. Karthik, P. Selvakumar, P. Senthil Kumar, D.-V. N. Vo, M. Gokulakrishnan, P. Keerthana, V. Tamil Elakkiya, and R. Rajeswari, "Graphene-based materials for environmental applications: a review," *Environmental Chemistry Letters*, vol. 19, no. 5, pp. 3631–3644, 2021.

[9] M. Han, Y. Muhammad, Y. Wei, Z. Zhu, J. Huang, and J. Li, "A review on the development and application of graphene based materials for the fabrication of modified asphalt and cement," *Construction and Building Materials*, vol. 285, p. 122885, 2021.

[10] E. Kymakis, E. Stratakis, M. Stylianakis, E. Koudoumas, and C. Fotakis, "Spin coated graphene films as the transparent electrode in organic photovoltaic devices," *Thin Solid Films*, vol. 520, no. 4, pp. 1238–1241, 2011.

[11] S. Novikov, N. Lebedeva, K. Pierz, and A. Satrapinski, "Fabrication and study of large-area qhe devices based on epitaxial graphene," *IEEE Transactions on Instrumentation and Measurement*, vol. 64, no. 6, pp. 1533–1538, 2015.

[12] B. Kiraly, R. M. Jacobberger, A. J. Mannix, G. P. Campbell, M. J. Bedzyk, M. S. Arnold, M. C. Hersam, and N. P. Guisinger, "Electronic and mechanical properties of graphene–germanium interfaces grown by chemical vapor deposition," *Nano letters*, vol. 15, no. 11, pp. 7414–7420, 2015.

[13] W. J. Hyun, E. B. Secor, M. C. Hersam, C. D. Frisbie, and L. F. Francis, "High-resolution patterning of graphene by screen printing with a silicon stencil for highly flexible printed electronics," *Advanced Materials*, vol. 27, no. 1, pp. 109–115, 2015.

[14] S. Novikov, A. Satrapinski, N. Lebedeva, and I. Iisakka, "Sensitivity optimization of epitaxial graphene-based gas sensors," *IEEE Transactions on Instrumentation and Measurement*, vol. 62, no. 6, pp. 1859–1864, 2013.

[15] M. Yuan, E. C. Alocilja, and S. Chakrabartty, "A novel biosensor based on silver-enhanced self-assembled radio-frequency antennas," *IEEE Sensors Journal*, vol. 14, no. 4, pp. 941–942, 2013.

[16] W. Su, J. Xu, and X. Ding, "An electrochemical ph sensor based on the amino-functionalized graphene and polyaniline composite film," *IEEE transactions on nanobioscience*, vol. 15, no. 8, pp. 812–819, 2016.

[17] X. Leng, W. Li, D. Luo, and F. Wang, "Differential structure with graphene oxide for both humidity and temperature sensing," *IEEE Sensors Journal*, vol. 17, no. 14, pp. 4357–4364, 2017.

[18] M. Sanaeepour, A. Abedi, and M. J. Sharifi, "Performance analysis of nanoscale single layer graphene pressure sensors," *IEEE Transactions on Electron Devices*, vol. 64, no. 3, pp. 1300–1304, 2017.

[19] M. Dragoman, D. Neculoiu, D. Dragoman, G. Deligeorgis, G. Konstantinidis, A. Cismaru, F. Coccetti, and R. Plana, "Graphene for microwaves," *IEEE Microwave Magazine*, vol. 11, no. 7, pp. 81–86, 2010.

[20] M. Bozzi, L. Pierantoni, and S. Bellucci, "Applications of graphene at microwave frequencies," *Radioengineering*, vol. 24, no. 3, pp. 661–669, 2015.

[21] L. Pierantoni, D. Mencarelli, M. Bozzi, R. Moro, S. Moscato, L. Perregrini, F. Micciulla, A. Cataldo, and S. Bellucci, "Broadband microwave attenuator based on few layer graphene flakes," *IEEE Transactions on Microwave Theory and Techniques*, vol. 63, no. 8, pp. 2491–2497, 2015.

[22] P. Savi, K. Naishadam, A. Bayat, M. Giorcelli, and S. Quaranta, "Multi-walled carbon nanotube thin film loading for tuning microstrip patch antennas," in *2016 10th European Conference on Antennas and Propagation (EuCAP)*. IEEE, 2016, pp. 1–3.

[23] M. Yasir, P. Savi, S. Bistarelli, A. Cataldo, M. Bozzi, L. Perregrini, and S. Bellucci, "A planar antenna with voltage-controlled frequency tuning based on few-layer graphene," *IEEE Antennas and wireless propagation Letters*, vol. 16, pp. 2380–2383, 2017.

[24] H. Jiao, K. Yang, S. Sang, Z. Pei, R. Guo, H. Shi, and W. Wang, "Graphene-based flexible temperature/pressure dual-mode sensor as a finger sleeve for robotic arms," *Diamond and Related Materials*, vol. 142, p. 110799, 2024.

[25] A. A. Basheer, "Graphene materials for fabrication of robots," *Materials Chemistry and Physics*, vol. 302, 2023.

[26] M. Yasir and P. Savi, "Commercial graphene nanoplatelets-based tunable attenuator," *Electronics Letters*, vol. 56, no. 4, pp. 184–187, 2020.

[27] M. Yasir, F. Peinetti, and P. Savi, "Correlation of transmission properties with glucose concentration in a graphene-based microwave resonator," *Micromachines*, vol. 14, no. 12, p. 2163, 2023.

[28] F. Peinetti, P. Savi, and S. Quaranta, "Circuit model for graphene screen-printed films," *URSI Radio Sci. Lett.*, vol. 5, no. 4, 2023.

[29] F. Peinetti, S. Quaranta, and P. Savi, "Screen-printed graphene film circuit model for microwave applications," in *IEEE EUROCON 2023-20th International Conference on Smart Technologies*. IEEE, 2023, pp. 547–551.